THE JOURNAL OF BIOLOGICAL CHEMISTRY VOL. 290, NO. 18, pp. 11246–11257, May 1, 2015

Compartmentalized Accumulation of cAMP near Complexes of Multidrug Resistance Protein 4 (MRP4) and Cystic Fibrosis Transmembrane Conductance Regulator (CFTR) Contributes to Drug-induced Diarrhea*[S]

Received for publication, August 15, 2014, and in revised form, March 10, 2015 Published, JBC Papers in Press, March 11, 2015, DOI 10.1074/jbc.M114.605410

Changsuk Moon[‡§], Weiqiang Zhang[§¶], Aixia Ren[§‖], Kavisha Arora[‡§], Chandrima Sinha[§], Sunitha Yarlagadda[‡§], Koryse Woodrooffe[‡], John D. Schuetz[**], Koteswara Rao Valasani[‡‡], Hugo R. de Jonge[§§], Shiva Kumar Shanmukhappa[‡], Mohamed Tarek M. Shata[¶¶], Randal K. Buddington[‖‖], Kaushik Parthasarathi[§], and Anjaparavanda P. Naren[‡§1]

From the [‡]Department of Pediatrics, Cincinnati Children's Hospital Medical Center, Cincinnati, Ohio 45229, the Departments of [§]Physiology and [¶]Pediatrics, University of Tennessee Health Science Center, Memphis, Tennessee 38163, the Departments of [‖]Hematology and [**]Pharmaceutical Sciences, St. Jude Children's Research Hospital, Memphis, Tennessee 38105, the [‡‡]Department of Pharmacology and Toxicology and Higuchi Bioscience Center, School of Pharmacy, University of Kansas, Lawrence, Kansas 66047, the [§§]Department of Gastroenterology and Hepatology, Erasmus University Medical Center, 3000CA Rotterdam, The Netherlands, the [¶¶]Division of Digestive Diseases, University of Cincinnati Medical Center, Cincinnati, Ohio 45267, and the [‖‖]Department of Health and Sport Sciences, University of Memphis, Memphis, Tennessee 38152

Background: Diarrhea is an adverse side effect associated with many therapeutics.
Results: Irinotecan induced hyperactive cystic fibrosis transmembrane conductance regulator (CFTR) function by inhibiting multidrug resistance protein 4 (MRP4) and formation of MRP4-CFTR macromolecular complexes.
Conclusion: MRP4-CFTR-containing macromolecular complexes play an important role in drug-induced diarrhea.
Significance: These studies help define molecular mechanisms of drug-induced diarrhea.

Diarrhea is one of the most common adverse side effects observed in ~7% of individuals consuming Food and Drug Administration (FDA)-approved drugs. The mechanism of how these drugs alter fluid secretion in the gut and induce diarrhea is not clearly understood. Several drugs are either substrates or inhibitors of multidrug resistance protein 4 (MRP4), such as the anti-colon cancer drug irinotecan and an anti-retroviral used to treat HIV infection, 3′-azido-3′-deoxythymidine (AZT). These drugs activate cystic fibrosis transmembrane conductance regulator (CFTR)-mediated fluid secretion by inhibiting MRP4-mediated cAMP efflux. Binding of drugs to MRP4 augments the formation of MRP4-CFTR-containing macromolecular complexes that is mediated via scaffolding protein PDZK1. Importantly, HIV patients on AZT treatment demonstrate augmented MRP4-CFTR complex formation in the colon, which defines a novel paradigm of drug-induced diarrhea.

Diarrhea is a common side effect of ~7% of all adverse drug reactions and results from impaired fluid secretion in the small and large intestine (1, 2). Fluid homeostasis and secretion in the intestine are driven by active Cl^- transport from the basolateral to the apical side of enterocytes (3). Multidrug resistance protein 4 (MRP4)[2] is a member of the ATP-binding cassette (ABC) transporter superfamily of proteins that has been shown to negatively regulate intracellular accumulation of drugs, such as nucleoside analogs that are in use for HIV treatment (4).

Irinotecan is used as both a first-line and a second-line chemotherapeutic drug for advanced and recurrent colon cancer (5). However, irinotecan induces severe diarrhea as a side effect, the onset of which can be either delayed or acute (6). The former is related to mucosal and colonic damage secondary to metabolism of irinotecan; however controversy remains regarding the mechanism of acute-onset diarrhea (7). The mechanism of acute-onset diarrhea has been attributed to irinotecan anticholinesterase activity (8), although up to 25% of patients do not exhibit changes in cholinesterase activity (9), and other studies suggest that irinotecan anticholinesterase does not account for increased fluid secretion (10).

In this study, we used complementary model systems to elucidate the mechanism of irinotecan-induced diarrhea, including *in vitro* mouse intestinal enteroid cultures (enterospheres) that mimic the physiological environment of the intestine. We demonstrate that drug inhibition of MRP4 (*e.g.* via the use of irinotecan or 3′-azido-3′-deoxythymidine (AZT)) produces compartmentalized accumulation of cAMP in close proximity to cystic fibrosis transmembrane conductance regulator

* The work was supported by National Institutes of Health Grants DK080834 and DK093045 (to A. P. N.) and GM060904 (to J. D. S.).
[S] This article contains supplemental Video 1.
[1] To whom correspondence should be addressed: Dept. of Pediatrics, Cincinnati Children's Hospital Medical Center, 3333 Burnet Ave., S-6322, Cincinnati, OH 45229. Tel.: 513-803-4731; Fax: 513-803-4783; E-mail: anaren@cchmc.org.

[2] The abbreviations used are: MRP4, multidrug resistance protein 4; CFTR, cystic fibrosis transmembrane conductance regulator; AZT, 3′-azido-3′-deoxythymidine; NVP, nevirapine; NRTI, nucleoside/nucleotide reverse transcriptase inhibitor; HBSS, Hanks' balanced salt solution; PMEA, poly (2-methoxyethyl acrylate); DMSO, dimethyl sulfoxide; PLA, proximity ligation assay; SPT, single-particle tracking; cpt-cAMP, 8-(4-chlorophenylthio)-cAMP.

(CFTR), which activates the CFTR channel function, causing excessive fluid secretion and diarrhea.

EXPERIMENTAL PROCEDURES

Mice and Cell Lines—Mrp4$^{-/-}$ mice were developed as described previously (11) and backcrossed for 10 generations with the C57BL6/sJ strain. Syngeneic C57BL/6 mice were obtained from Charles River (Wilmington, MA). The polarized human gut epithelial cell line, HT29-CL19A, was purchased from the American Type Culture Collection (Manassas, VA), and FLAG-MRP4-overexpressing HT29-CL19A cells were generated by stable transfection with pLenti PGK Puro-FLAG-MRP4.

Measurement of Intestinal Fluid Secretion in Mice—Intestinal fluid secretion measurement in murine ileal loops was performed as described previously (12). Three ileal loops were made on the ileum between 0.5 and 3.5 cm from the cecum, between the jejunum and the cecum, and each closed loop was injected with PBS-diluted DMSO, 0.5 μg of cholera toxin (Sigma-Aldrich), or 4–100 μM irinotecan (Sigma-Aldrich). Intestinal loops were removed from the mice 6 h after the operation, and the length and weight of each loop including fluid were measured. After drying each loop for 24 h, the weight of the loops was measured again, and the weight of fluid was calculated for each loop and divided by the length of the loop to determine the amount of fluid secretion.

Isolation and Culture of Intestinal Crypts and Enteroids—The entire small intestine was removed from 8-week-old mice and washed with cold PBS. After opening the small intestine, villi were discarded by scraping with a cover slide, and the tissue was cut into small pieces. After washing with cold PBS several times, the pieces of tissue were incubated at 4 °C in PBS containing 2 mM EDTA for 30 min and then passed through a 70-μm cell strainer. The crypts were collected by centrifugation at 1,200 rpm for 5 min and cultured on Matrigel (BD Biosciences) with organoid medium (Advanced DMEM/F12 (Gibco®) supplemented to contain 1× GlutaMAX (Gibco®), 1× penicillin (Gibco®), 1× streptomycin (Gibco®), 10 mM HEPES (Gibco®), 1× B27 (Gibco®), 1× N2 (Gibco®), 1 mM *N*-acetyl-L-cysteine (Sigma-Aldrich), 100 ng/ml noggin (PeproTech, Crescent Ave Rocky Hill, NJ), 1 μg/ml R-spondin-1 (R&D Systems, Minneapolis, MN), 50 ng/ml EGF (R&D Systems)) in a humidified 10% CO_2 incubator at 37 °C for 30 min (13–15).

Measurement of Fluid Secretion in Intestinal Enterospheres—Matrigel-embedded enterospheres were placed with Hanks' balanced salt solution (HBSS) into glass-bottomed dishes (MatTek, Ashland, MA). The following were added: DMSO (Sigma-Aldrich), 0–100 μM irinotecan, 50 μM MK-571 (Cayman, Ann Arbor, MI), 0–10 μM forskolin (Tocris, Bristol, UK), 100 μM doxorubicin (Bedford Laboratories, Bedford, OH), 0–10 μM AZT (Sigma-Aldrich), or 0–10 μM nevirapine (NVP (Sigma-Aldrich))) with or without 20 μM of the CFTR inhibitor CFTRinh-172 or 0–0.5 μM atropine (Sigma-Aldrich). Enterospheres were incubated at 37 °C for 30 min, and images were obtained using a phase-contrast IX-51 microscope (Olympus, Tokyo, Japan). The radii of the luminal sphere and the entire enterosphere sphere were measured using the ImageJ software (rsbweb.nih.gov/ij/), and the ratios between the volume of the luminal sphere and the entire sphere were calculated to determine fluid secretion.

Two-photon Three-dimensional Images of Enterospheres and Enteroids—To prepare specimens, formalin-fixed enterospheres and enteroids were put into HistoGel (AMTS; Lodi, CA) and stained with propidium iodide. Fluorescence images were obtained at various depths within the sample using Z-stacks on an LSM 710 laser-scanning confocal microscope (Carl Zeiss; Thornwood, NY). Three-dimensional images were created using images of various planes and the ZEN Imaging Software (Carl Zeiss).

Immunohistochemistry—After fixing with 4% formalin, the mouse small intestine and enterospheres were embedded in paraffin and sectioned. For immunofluorescence staining, enterospheres were directly fixed on glass-bottomed dishes with 4% formalin. The samples were permeabilized and blocked and then incubated with CFTR (anti-CFTR rabbit polyclonal antibody R3194 (16)) and MRP4 (anti-MRP4 rabbit polyclonal antibody (11)) antibodies. Rabbit IgG (normal rabbit IgG: Santa Cruz Biotechnology, Santa Cruz, CA) was used as a negative control. The samples were then treated with Alexa Fluor® 488-conjugated anti-rabbit antibody (Invitrogen) and propidium iodide. Fluorescence images were taken on an LSM 5 PASCAL confocal laser scanning microscope (Carl Zeiss).

Short-circuit Current (I_{SC}) Measurement—I_{SC} values were measured in polarized HT29-CL19A cells mounted in a modified Ussing chamber as described previously (17). Irinotecan (50 μM) was added to both the apical and the basolateral sides for 10 min before cpt-cAMP (50 μM; Sigma-Aldrich) was added to both the apical and the basolateral sides to activate CFTR channels. CFTRinh-172, (20 μM), which is a specific CFTR channel blocker, was added to the apical side.

Western Blot—After homogenization of cells or tissues with lysis buffer (PBS containing 0.2% Triton X-100, 1 mM phenylmethylsulfonyl fluoride, 1 μg/ml pepstatin A, 1 μg/ml leupeptin, 1 μg/ml aprotinin), the lysates were separated on 4–15% gradient SDS-polyacrylamide gels. Separated proteins were electrophoretically transferred onto PVDF membrane, blotted, and probed for proteins of interest using specific antibodies: MRP4 (anti-MRP4 rabbit polyclonal antibody), CFTR (anti-CFTR rabbit polyclonal antibody R3194), PDZK1 (anti-PDZK1 rabbit polyclonal antibody (18)), and β-actin (anti-β-actin mouse monoclonal antibody; Sigma-Aldrich). The protein bands were detected using ECL™ Western blot detection reagents (GE Healthcare, Buckinghamshire, UK).

Measurement of Intracellular cAMP Levels—HT29-CL19A cells were treated with DMSO, 100 μM irinotecan, 50 μM MK-571, or 10 μM forskolin in HBSS and incubated at 37 °C for 10 min. After incubation, the cells were washed with cold PBS and harvested. For enterospheres from *Mrp4*$^{+/+}$ mice, after removing Matrigel from the enterosphere culture, enterospheres were placed into 1.5-ml tubes with HBSS and humidified in a 10% CO_2 incubator at 37 °C for 30 min. Subsequently, DMSO, 100 μM irinotecan, 50 μM MK-571, or 10 μM forskolin was added, and the enterospheres were stimulated at 37 °C for 10 min. Intracellular cAMP concentrations were determined using a cAMP complete ELISA kit (Enzo, Farmingdale, NY) according to the manufacturer's instructions. The values of

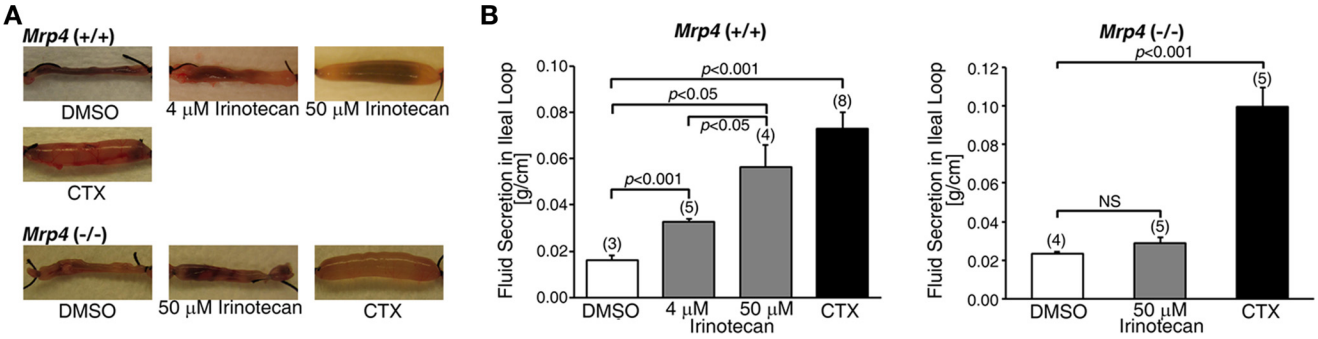

FIGURE 1. **Irinotecan induced fluid secretion in ileal loops from *Mrp4*$^{+/+}$ but not *Mrp4*$^{-/-}$ mice.** *A*, representative images of ileal loops from the small intestine of *Mrp4*$^{+/+}$ and *Mrp4*$^{-/-}$ mice. The loops were injected with DMSO, irinotecan, or cholera toxin (*CTX*: positive control). Irinotecan induced fluid secretion in *Mrp4*$^{+/+}$ mice in a dose-dependent manner, but failed to induce fluid secretion in *Mrp4*$^{-/-}$ mice. *B*, data quantified from experiments as represented in *panel A*. Data are presented as mean ± S.E. *NS*, not significant ($p \geq 0.05$).

cAMP levels were normalized to the total protein concentration.

[^{3}H]PMEA Efflux Assay—HT29-CL19A cells were incubated with 10 μM [^{3}H]PMEA (Moravek, Brea, CA) in serum-free DMEM at 37 °C for 24 h. After washing with warm PBS, 2 ml of serum-free DMEM containing DMSO, 0–100 μM irinotecan, or 50 μM MK-571 were added to the cells. During incubation at 37 °C for 30 min, 0.5-ml culture supernatants were collected every 10 min to measure the efflux of [^{3}H]PMEA, and the cells were lysed with 0.1 N NaOH in 0.5% SDS to measure the residual intracellular [^{3}H]PMEA. The amount of radioactivity was determined on a Tri-Carb liquid scintillation counter (PerkinElmer). The values of intracellular [^{3}H]PMEA were normalized by dividing by the total protein concentration of cell lysates.

[^{3}H]cAMP Transporter Assay—HT29-CL19A cells were mounted on Transwell permeable supports (BD Biosciences) until the transepithelial resistance reached more than 1,500 ohms. The cell monolayers were permeabilized at the basolateral side using 100 μg/ml α-toxin (Calbiochem) to allow the entry of [^{3}H]cAMP (PerkinElmer). To inhibit MRP4, cells were incubated with 100 μM irinotecan or 50 μM MK-571 in HBSS both apically and basolaterally at 37 °C for 30 min. 1 μCi/ml [^{3}H]cAMP (PerkinElmer) and 4 mM Mg-ATP were added at the basolateral side, and cells then were incubated at 37 °C for 30 min, after which samples were collected from the apical side. The amount of radioactivity was measured on a Tri-Carb liquid scintillation counter. Cells without permeabilization at the basolateral side were used as a control.

FRET Assay—FRET was used to measure real-time changes in intracellular cAMP. HT29-CL19A cells expressing a cAMP sensor, CFP-EPAC-YFP, were grown on glass-bottomed dishes, washed twice with HBSS, and stimulated with DMSO, 100 μM irinotecan, or 10 μM forskolin. Ratiometric FRET imaging and data analysis were performed as described previously (18).

Single-particle Tracking (SPT)—To measure the diffusion constant of MRP4 on the plasma membrane, a quantum (Q)-dot labeling method was used (19). We generated a fully functional FLAG-tagged MRP4 construct on the fourth outer loop (between Gly-751 and Gly-752) facing the extracellular surface. HT29-CL19A cells stably expressing FLAG-MRP4 were used for SPT as described previously (17). After incubating with biotin-conjugated anti-FLAG antibody (Sigma-Aldrich) and streptavidin-conjugated Qdot-655 (Invitrogen) in sequence, images were captured 10 min after treating with DMSO, 100 μM irinotecan, or 10 μM forskolin.

Pulldown Assay—MRP4-overexpressing HT29-CL19A cells were stimulated with DMSO or 0–100 μM irinotecan for 10 min. The cell lysates were mixed with purified GST or GST-PDZK1 and immunoprecipitated using glutathione-agarose beads (Sigma-Aldrich). The immunoprecipitated beads were washed three times with lysis buffer containing DMSO or 0–100 μM irinotecan, and the proteins were eluted from the beads using 5×Laemmli sample buffer containing 2.5% β-mercaptoethanol. The eluted samples were immunoblotted for MRP4 (anti-MRP4 rabbit polyclonal antibody), and the band intensity was quantified using ImageJ software.

The in Situ Proximity Ligation Assay (PLA)—Enterospheres were cultured in glass-bottomed dishes and stimulated with 100 μM irinotecan at 37 °C for 10 min. Immunocytochemistry was performed using antibodies for MRP4 (anti-MRP4 rabbit polyclonal antibody) and CFTR (anti-CFTR mouse monoclonal antibody; CF3, Abcam, Cambridge, MA). To measure PLA signals, we used Duolink reagents (Olink Biosciences, Uppsala, Sweden) according to the manufacturer's instructions (20). PLA signals were detected on an LSM 5 PASCAL confocal laser scanning microscope. The intensities of the PLA signals (*i.e.* the affinity of the interaction) were quantified using the ImageJ software.

The in Silico Topological Study for Docking of Irinotecan into MRP4—The three-dimensional structure of MRP4 isoenzymes was constructed by the homology modeling method (12). Each MRP4 isoenzyme sequence was derived from BLAST (blast.ncbi.nlm.nih.gov/Blast.cgi), and the crystal structure of P-glycoprotein was chosen as the template (Protein Data Base ID: 3G60). A sequence alignment file was generated by ClustalX, and the three-dimensional model of MRP4 was predicted using the Modeller 9v8 tool. The three-dimensional structure of irinotecan was constructed in the Molecular Operating Environment. The interaction of irinotecan in the binding domain cavity of MRP4 was analyzed from a ligand-interaction study of the Molecular Operating Environment (21–23).

Statistical Analysis—The data are expressed as mean ± S.E. One-way analysis of variance was used to compare multiple groups, and Student's *t* test was used for intergroup comparisons. Statistical significance was designated as $p \leq 0.05$. All data

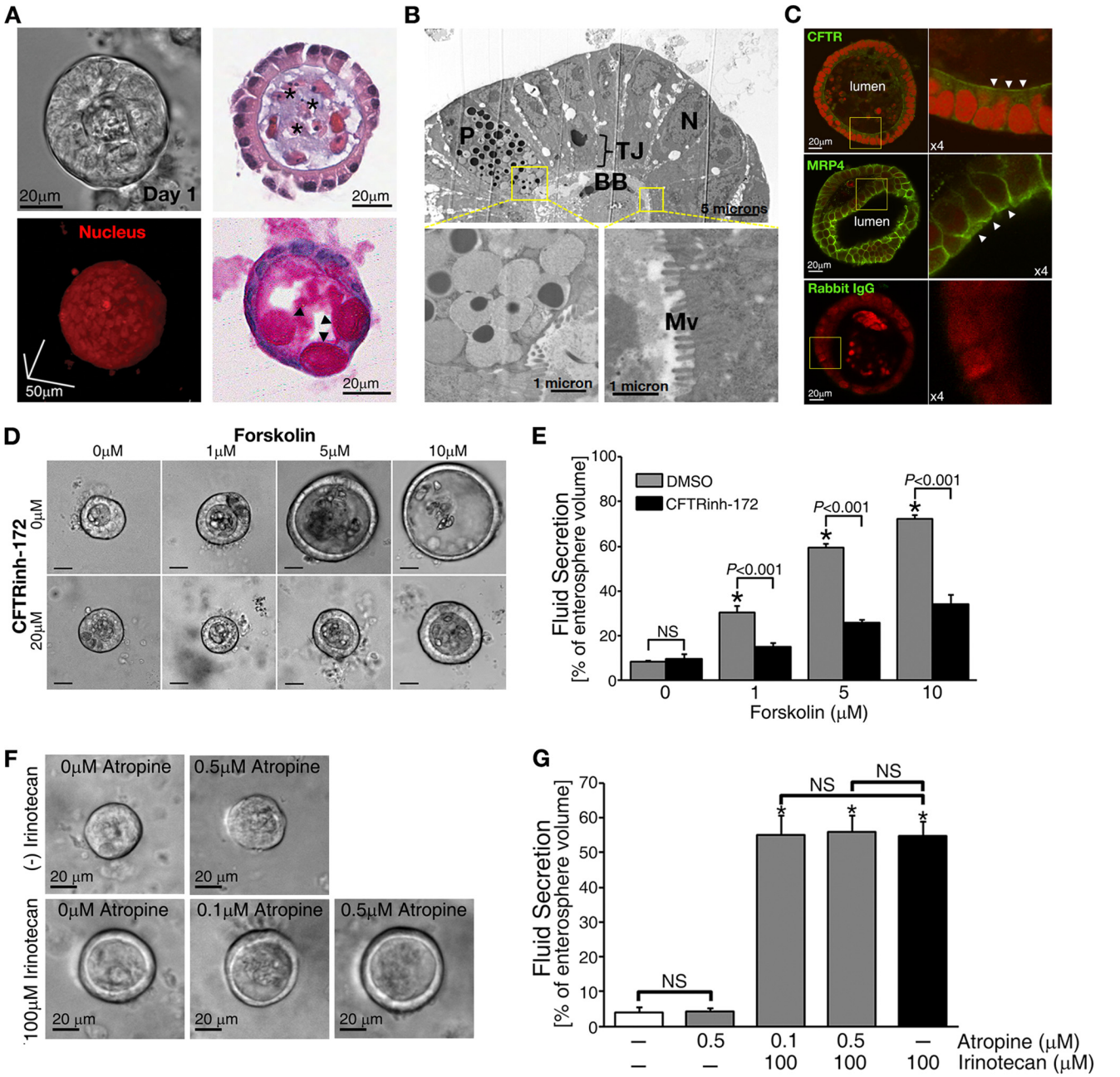

FIGURE 2. **Enterospheres developed from the small intestine of adult mice showed robust CFTR-mediated fluid secretion.** *A*, representative phase-contrast image (*upper left*) and two-photon micrograph of a three-dimensional cultured enterosphere in Matrigel (*lower left*). *Upper right*, histological analysis of enterospheres by HE staining; *lower right*, periodic acid/Schiff staining. *, luminal area. *Arrowheads* indicate goblet cells in the enterosphere. *B*, electron microscope micrographs showing paneth cell (*P*), brush border (*BB*), and microvilli (*Mv*) in the enterosphere (*TJ*: tight junction; *N*: nuclei). *C*, immunohistochemistry staining showing the apical (indicated by *arrowheads*) localization of CFTR and MRP4 on the enterosphere. Rabbit IgG is used as a negative control. *D*, forskolin treatment induced CFTR-mediated fluid secretion into the luminal area of the enterospheres in a dose-dependent manner. A specific CFTR channel blocker, CFTRinh-172, inhibited the secretion. *Scale bars* = 20 μm. *E*, the data were quantified from experiments as represented in Fig. 1*D*. *F*, representative phase-contrast images of fluid secretion in enterospheres from *Mrp4*$^{+/+}$ mice in response to irinotecan with or without atropine, an anticholinergic agent. Atropine did not affect irinotecan-increased fluid. *G*, the data were quantified from experiments as represented in Fig. 1*F*. All fluid secretion data from enterospheres are presented as the mean ± S.E. ($n \geq 10$ enterospheres per group). At least three individual experiments were performed using different mice. *, significant difference as compared with 0 μM irinotecan-treated without atropine group; *NS*, not significant ($p \geq 0.05$).

were analyzed using Microsoft Office 2010 (Microsoft, Redmond, WA).

RESULTS

Mrp4$^{-/-}$ *Mice Are Resistant to Irinotecan-induced Fluid Secretion*—We evaluated the effect of irinotecan (4 and 50 μM) on intestinal fluid secretion in wild-type (*Mrp4*$^{+/+}$) and *Mrp4*$^{-/-}$ mice using a closed-loop diarrhea model (12). DMSO (the solvent for irinotecan) was used as a negative control, and cholera toxin (0.5 μg/loop), which activates CFTR-mediated fluid secretion, was used as a positive control. Irinotecan treatment significantly increased fluid secretion in ileal loops from *Mrp4*$^{+/+}$ mice in a dose-dependent manner (2-fold increase (4 μM) and 3.47-fold increase (50 μM) *versus* DMSO in *Mrp4*$^{+/+}$), but had no effect on

fluid secretion in *Mrp4*$^{-/-}$ mice (Fig. 1, *A* and *B*). The data indicate a role for MRP4 in irinotecan-induced intestinal fluid secretion that manifests as diarrhea.

Development of Adult Mouse intestinal Enterosphere System to Study Mechanisms of Drug-induced Diarrhea—To test whether MRP4-CFTR-coupled complexes are involved in iri-

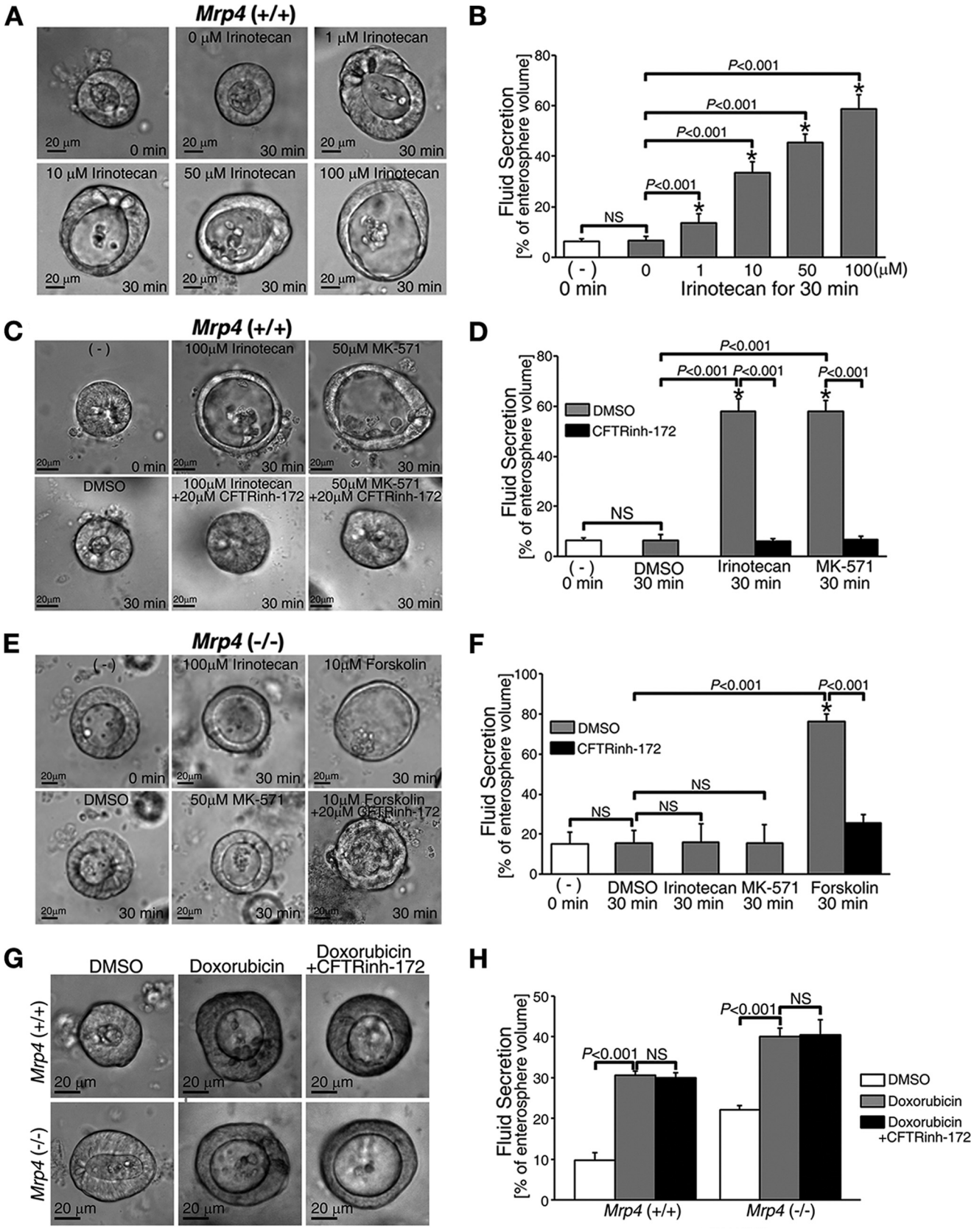

notecan-induced diarrhea, we developed a physiologically relevant system that mimics the native intestine (13, 24–26). Crypts were isolated and purified from the small intestine of adult mice and cultured in Matrigel for three-dimensional growth to form enterospheres (Fig. 2*A*). Central lumen and brush-border structures found in enterospheres were visualized (Fig. 2, *A* and *B*) (27, 28). CFTR was localized mostly to the apical membrane with MRP4 present at both the apical and the basolateral surfaces (Fig. 2*C*) (4, 16). The cultured enterospheres provide a physiologically relevant model to study CFTR-dependent intestinal fluid secretion in culture (Fig. 2, *D* and *E*). The clinically relevant concentration of an anticholinergic agent, atropine (0.2–0.4 mg/kg) (29), did not cause a significant inhibition of irinotecan-induced fluid secretion (Fig. 2, *F* and *G*). Therefore, the observed lack of cholinergic neurons demonstrates that cholinergic effects are excluded in enterospheres.

Irinotecan Augments CFTR-mediated Fluid Secretion in Enterospheres from Wild-type Mrp4$^{+/+}$ Mice, but Not from Mrp4$^{-/-}$ Mice—We successfully reproduced the role of MRP4 in irinotecan-induced fluid secretion in enterospheres (Fig. 3, *A–F*, comparable with *in vivo* data shown in Fig. 1, *A* and *B*). Irinotecan-induced fluid was secreted significantly in enterospheres from *Mrp4*$^{+/+}$ mice in a dose-dependent manner (Fig. 3, *A* and *B*). Of note, clinically relevant concentrations in the serum of patients receiving irinotecan are reported to be in the range of ~2–4 μM (30, 31). Importantly, irinotecan-induced fluid secretion was CFTR-dependent because CFTRinh-172 completely inhibited fluid secretion and, as expected, MK-571 (an inhibitor of MRP4) also induced CFTR-mediated fluid secretion (Fig. 3, *C* and *D*). Neither irinotecan nor MK-571 induced fluid secretion, whereas forskolin, which increases intracellular cAMP, did induce CFTR-mediated fluid secretion in enterospheres from *Mrp4*$^{-/-}$ mice (Fig. 3, *E* and *F*, supplemental Video 1).

To investigate the specificity of MRP4 and CFTR in irinotecan-induced intestinal fluid secretion, we tested doxorubicin, another anti-colon cancer drug that has been reported to cause diarrhea during chemotherapy and is not a modulator for MRP4 (32). We found that following 30 min of treatment, doxorubicin induced similar fluid secretion rates in enterospheres from *Mrp4*$^{+/+}$ and *Mrp4*$^{-/-}$ mice (~20%), and CFTRinh-172 did not inhibit such secretion (Fig. 3, *G* and *H*). These studies suggest that doxorubicin-induced diarrhea is independent of MRP4. More importantly, our studies suggest that doxorubicin-induced fluid secretion is unlikely to be mediated by CFTR Cl^- channels.

Irinotecan Activates CFTR Chloride Channel Function via Increasing Intracellular cAMP Levels by Altering MRP4 Function—To define a mechanism underlying drug-induced fluid secretion, we monitored CFTR-dependent I_{SC} (an indicator of transepithelial Cl^- transport) in polarized HT29-CL19A cells that endogenously express CFTR and MRP4 (18). We observed a significant increase in CFTR-mediated I_{SC} in irinotecan-pretreated cells as compared with control DMSO-pretreated cells in response to a submaximal stimulation of the channel (*i.e.* 50 μM cpt-cAMP; Fig. 4, *A* and *B*). The maximal CFTR-mediated I_{SC} in irinotecan-pretreated samples was 2.5-fold higher as compared with the controls (Fig. 4*B*).

Given that irinotecan has been reported to be a substrate for MRP4 (33) and MRP4 is an efflux pump for cAMP and cGMP (34), we reasoned that irinotecan might alter intracellular cAMP levels. Indeed, irinotecan elevated intracellular cAMP to levels comparable with the effect of MK-571 in HT29-CL19A cells and mouse intestinal enterospheres (Fig. 4, *C* and *D*). Using a FRET-based cAMP sensor (CFP-EPAC-YFP), we found that irinotecan evoked a significant increase in cAMP levels at or near the plasma membrane, whereas forskolin induced uniform cAMP signals throughout the cell (Fig. 4, *E* and *F*).

We tested whether irinotecan-induced accumulation of intracellular cAMP is caused by inhibition of MRP4 function. Using [^{3}H]PMEA, which is a specific substrate for MRP4 (35), to perform transport studies for MRP4, we found that [^{3}H]PMEA efflux was inhibited by irinotecan in a dose-dependent manner as compared with vehicle-treated controls (Fig. 4*G*). We also monitored the MRP4-mediated unidirectional transport of [^{3}H]cAMP across the apical membrane of polarized HT29-CL19A cells and observed that both irinotecan and MK-571 inhibited the MRP4-mediated transport of [^{3}H]cAMP by more than 40% as compared with the DMSO-vehicle control (Fig. 4*H*). These results suggest that irinotecan can alter MRP4 function on the apical plasma membrane surface and thereby block cAMP efflux.

Binding of Irinotecan to MRP4 Augments Its Interaction with PDZ Proteins—Given that membrane-spanning proteins have a defined diffusion property (lateral mobility) at the plasma membrane and formation of multiprotein complexes will restrict or immobilize their diffusion property in live cells (17), we used SPT to track the trajectories of Q-dot-labeled FLAG-MRP4 in live HT29-CL19A cells with or without irinotecan

FIGURE 3. **Irinotecan induced fluid secretion in enterospheres from *Mrp4*$^{+/+}$ mice in a dose-dependent manner.** Conversely, enterospheres from *Mrp4*$^{-/-}$ mice were resistant to irinotecan-induced fluid secretion. *A*, representative phase-contrast images showing fluid secretion in enterospheres from *Mrp4*$^{+/+}$ mice in response to irinotecan. Irinotecan induced fluid secretion in a dose-dependent manner. *B*, quantification of data from experiments as represented in *panel A*. *C*, representative phase-contrast images showing fluid secretion in enterospheres from *Mrp4*$^{+/+}$ mice in response to irinotecan with or without CFTRinh-172, a CFTR channel blocker. MK-571, an MRP4 inhibitor, was used as a positive control. The irinotecan-induced fluid secretion in enterospheres from *Mrp4*$^{+/+}$ mice was CFTR-mediated. *D*, quantification of data from experiments as represented in *panel C*. *E*, representative phase-contrast images showing fluid secretion in enterospheres from *Mrp4*$^{-/-}$ mice in response to irinotecan, forskolin, or MK-571. Irinotecan and MK-571 failed to induce fluid secretion in these enterospheres. *F*, quantification of data from experiments as represented in *panel E*. *G*, representative phase-contrast images of fluid secretion in enterospheres from *Mrp4*$^{+/+}$ and *Mrp4*$^{-/-}$ mice in response to the anti-cancer drug doxorubicin with or without CFTRinh-172. Doxorubicin, which induces diarrhea during chemotherapy and is not a modulator for MRP4, induced a similar fluid secretion rate in enterospheres from *Mrp4*$^{+/+}$ and *Mrp4*$^{-/-}$ mice (~2-fold higher as compared with the basal level of secretion in each group) and CFTRinh-172 did not inhibit doxorubicin-induced fluid secretion. *H*, quantification of data from experiments as represented in *panel G*. In all bar graphs, the values represent the mean ± S.E. ($n \geq 10$ enterospheres per group), and at least three individual experiments were performed using different mice in each panel. *, significant difference from unstimulated group (0 min); *NS*, not significant ($p \geq 0.05$).

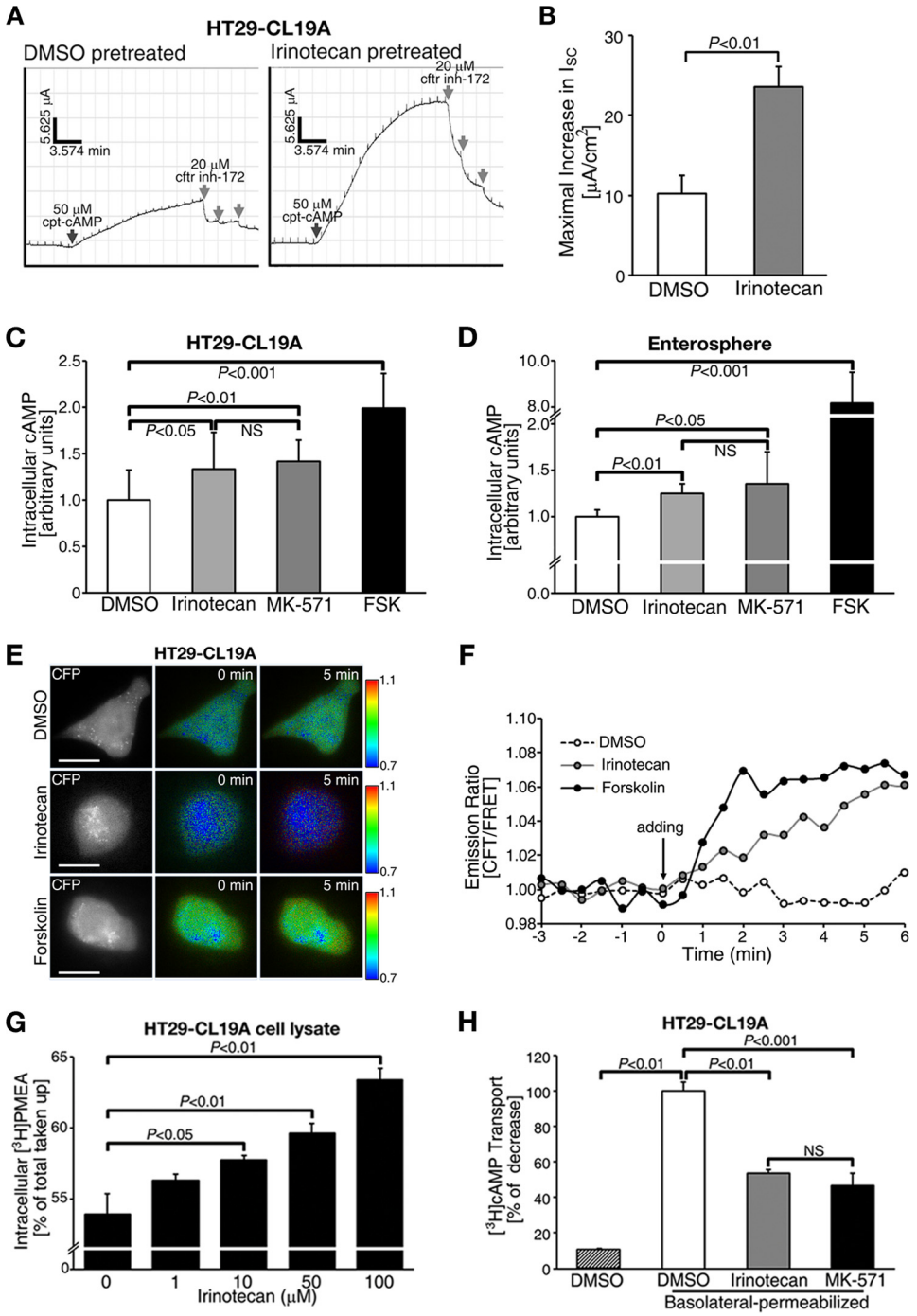

FIGURE 4. **Irinotecan augmented CFTR-mediated transepithelial Cl^- transport by inhibiting the MRP4 efflux pump, thus elevating intracellular cAMP levels at or near the plasma membrane.** *A*, representative traces of CFTR-mediated short-circuit currents (I_{SC}) in response to cpt-cAMP in HT29-CL19A cells pretreated with irinotecan or vehicle (DMSO). *Black arrows* indicate the addition of cpt-cAMP to activate CFTR; *gray arrows* indicate the addition of CFTRinh-172. *B*, quantification of the CFTR-mediated maximal increase in I_{SC} from experiments as represented in *panel A*. *C*, irinotecan and MK-571 increased intracellular cAMP levels in HT29-CL19A cells. *D*, irinotecan and MK-571 increased intracellular cAMP levels in freshly isolated crypts from *Mrp4*$^{+/+}$ mice. *E*, pseudocolor images showing the changes in CFP/FRET emission ratio in HT29-CL19A cells expressing a cAMP sensor (CFP-EPAC-YFP) in response to DMSO, irinotecan, or forskolin. Irinotecan elevated cAMP levels at or near the plasma membrane, whereas forskolin induced a global cAMP response. The fluorescence images were captured from the same field of view. *Lookup bars* indicate the magnitude of the emission ratio. *F*, representative line graph showing the changes in CFP/FRET emission ratio in response to DMSO, irinotecan, or forskolin. The *arrow* indicates the addition of DMSO, irinotecan, or forskolin. The values are representative data in *panel E*. *G*, irinotecan inhibited the efflux of [^{3}H]PMEA in a dose-dependent manner in HT29-CL19A cells. *H*, irinotecan inhibited MRP4-mediated unidirectional transport of [^{3}H]cAMP across the apical plasma membrane of HT29-CL19A cells. The cells were permeabilized at the basolateral side. MK-571 was used as a positive control. In all bar graphs, the values represent the mean ± S.E. ($n \geq 3$ independent experiments in each group). *NS*, not significant ($p \geq 0.05$).

treatment. We found that irinotecan significantly decreased MRP4 diffusion at the plasma membrane as indicated by the trajectories (Fig. 5*A*, *upper panel*, and 5*B*) and the left shift of the distribution of diffusion coefficients (Fig. 5*A*, *lower panel*), suggesting that irinotecan enhances a macromolecular complex assembly of MRP4. Because MRP4 can form macromolec-

ular complexes via its C-terminal PDZ binding motif (36, 37), we next tested whether the PDZ motif of MRP4 plays a role in the irinotecan-induced decrease of MRP4 diffusion at the plasma membrane (upon irinotecan treatment). We generated an MRP4 construct that substitutes the PDZ motif TAL with AAA (named as ΔPDZ-MRP4 in this study) using site-directed mutagenesis (Fig. 5*C*). This mutant MRP4 does not binding to PDZ domain-containing proteins (18). We transfected the ΔPDZ-MRP4 into HT29-CL19A cells and tested the effect of irinotecan on MRP4 diffusion using SPT. The result demonstrates that irinotecan did not decrease MRP4 diffusion (Fig. 5*D*), supporting our hypothesis that irinotecan-induced slower wild-type MRP4 diffusion is a result of the complex formation between CFTR and MRP4. To investigate the effect of irinotecan on the CFTR-MRP4 interaction, we performed the PLA with the polarized HT29-CL19A cells transiently transfected with either wild-type MRP4 or ΔPDZ-MRP4. The PLA data clearly demonstrated irinotecan induced wild-type MRP4-

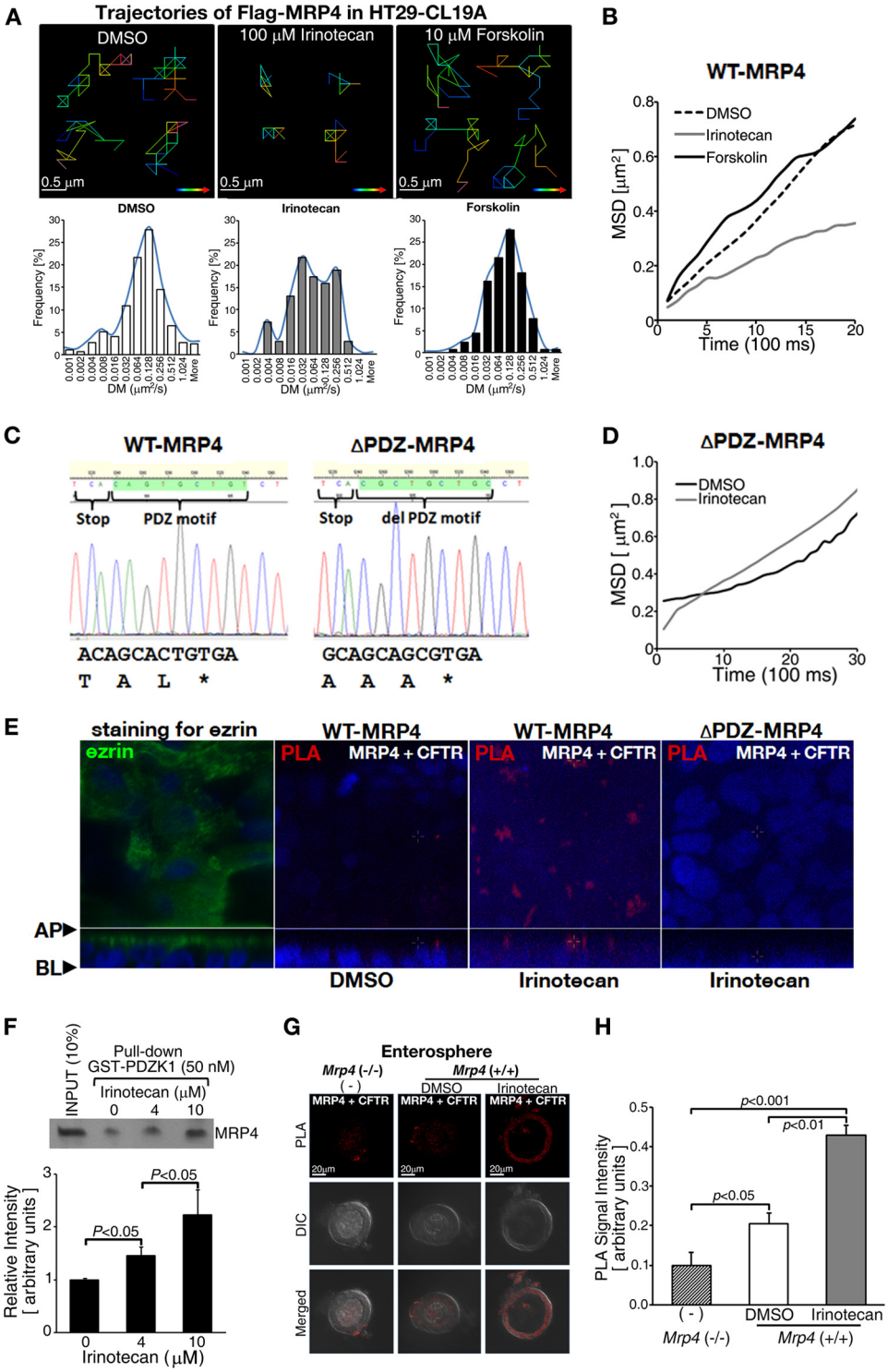

CFTR complex formation, but not ΔPDZ-MRP4-CFTR complex formation (Fig. 5*E*). Taken together, our data support the hypothesis that irinotecan induces complex formation between CFTR and wild-type MRP4 through PDZ motif-mediated interactions.

We next performed pulldown assays to determine whether irinotecan influences the interaction of MRP4 with its scaffolding partner PDZK1 and found that irinotecan does enhance the interaction (Fig. 5*F*). We also used an *in situ* PLA to examine whether irinotecan affects MRP4-CFTR interaction in cultured intestinal enterospheres. Treatment with irinotecan resulted in an additive increase (2.3-fold) in PLA signals of MRP4-CFTR interaction as compared with treatment with DMSO (Fig. 5, *G* and *H*).

FDA-approved Drugs (e.g. AZT) Augment the Formation of MRP4-CFTR-containing Macromolecular Complexes—The Food and Drug Administration (FDA) has approved several HIV drugs for the treatment of HIV, including the nucleoside/nucleotide reverse transcriptase inhibitors (NRTIs), which are substrates for MRP4 (4). The most common side-effect associated with NRTIs is diarrhea (38). Also, MRP4 transports AZT and the overexpression of MRP4 confers AZT resistance (4). To demonstrate the broad implications of our findings, we tested whether AZT induces diarrhea by activating MRP4-CFTR-containing macromolecular complexes using cultured intestinal enterospheres. NVP, which belongs to the non-NRTIs (NNRTIs) class of HIV drugs, was used as a negative control. We found that AZT induced CFTR-mediated fluid secretion in a dose-dependent manner and NVP did not induce fluid secretion (Fig. 6, *A* and *B*). The data demonstrate that the activation of MRP4-CFTR-containing macromolecular complexes might be a common mechanism for drug-related diarrhea. We also used the PLA to test whether AZT augments MRP4-CFTR macromolecular complex formation in enterospheres. Our data show that PLA signals were higher in AZT-treated enterospheres than in NVP-treated enterospheres (Fig. 6, *C* and *D*). To demonstrate the clinical relevance of this study, we used the PLA on colon from HIV patients and determined that MRP4-CFTR-containing macromolecular complexes were 2.17-fold higher in HIV-infected patients who were receiving AZT therapy as compared with normal controls (Fig. 6, *E* and *F*).

Binding of Irinotecan to MRP4 Induces Conformational Change in MRP4—The novelty of this study is the identification and characterization of a transporter-dependent pathway that is a key effector in the pathogenic process of drug-induced diarrhea. We demonstrated that drug-induced inhibition of MRP4 (*e.g.* via irinotecan or AZT) produces compartmentalized accumulation of cAMP in close proximity to CFTR and activates CFTR channel function, rapidly causing fluid secretion and diarrhea (Fig. 7). In summary, we have discovered a new molecular mechanism by which irinotecan causes secretory diarrhea (data summarized in Fig. 7*A*; *in silico* docking of MRP4 and irinotecan).

DISCUSSION

In this study, we found that CFTR-MRP4-containing macromolecular complexes played an important role in the pathogenesis of drug-induced diarrhea. Our findings have important and broad clinical implications because our model system can be used to identify novel agents that mitigate drug-induced diarrhea. Furthermore, our findings expand the concept that compartmentalized signaling (in this case, compartmentalized cAMP signaling) plays an important role in drug-induced pathophysiologic conditions (*e.g.* CFTR-dependent drug-induced diarrhea). These studies previously were not possible without the state-of-the-art methodology we have developed to define CFTR-mediated fluid secretion in cultured enterospheres. Because the enterospheres physiologically and structurally mimic the small intestine, this experimental system can be tailored to study additional pathophysiological conditions of the gastrointestinal tract.

The limitations in investigating the role of CFTR in secretory pathologies in intestine include the inaccessibility of crypt epithelial cells *in vivo* and dedifferentiation of intact crypt epithelia in primary cultures *ex vivo*. Recent studies using murine intestinal stem cells have yielded primary intestinal cultures in three-dimensional gel suspension that recapitulate crypt structure and epithelial differentiation (Fig. 2, *A* and *B*) (13, 14). For our studies, we used a modification of this model to evaluate the role of macromolecular complexes containing both MRP4 and CFTR in drug-induced diarrhea (Fig. 3, *A*–*H*, and supplemental Video 1).

Competitive irinotecan inhibition of cAMP efflux through MRP4 resulted in an increase in intracellular cAMP levels (Fig. 4, *C*–*F*). More importantly, this increase in cAMP was compartmentalized at or near the plasma membrane, suggesting that irinotecan increases cAMP levels by altering MRP4 function and thus inducing localized accumulation of cAMP (Fig. 4,

FIGURE 5. **Irinotecan enhanced the formation of MRP4-CFTR-containing macromolecular complexes at or near the plasma membrane by increasing the interaction between MRP4 and its binding PDZ protein, PDZK1.** *A*, SPT of FLAG-MRP4 at the plasma membrane. Irinotecan induced a significant decrease of lateral diffusion of MRP4 at the plasma membrane. *Upper* and *lower panels*, representative pseudocolor images showing the trajectories of MRP4 in cells treated with DMSO, irinotecan, or forskolin (*upper panels*) and distribution of diffusion coefficients (*DM*) for MRP4 particle trajectories (*lower panels*). *Lookup bars* indicate the direction of single particle movement (from blue to red). The experiments in each group were performed at least three times, and each individual group had significant differences as compared with the DMSO-treated group ($p < 0.05$). *B*, representative mean-squared displacement kinetics (*MSD*) of FLAG-MRP4 calculated from SPT experiments of DMSO-, irinotecan-, or forskolin-pretreated HT29-CL19A cells. *C*, DNA sequencing chromatogram showing the C-terminal PDZ motif of wild-type MRP4 and alanine substitution sequences of ΔPDZ-MRP4. *D*, representative mean-squared displacement kinetics of FLAG-ΔPDZ-MRP4 calculated from SPT experiments of DMSO- or irinotecan-pretreated HT29-CL19A cells. *E*, confocal images showing PLA signals (*red*) between MRP4 and CFTR in wild-type MRP4 or ΔPDZ-MRP4-overexpressing HT29-CL19A cells. The cells were polarized and treated with DMSO or irinotecan at the apical side. Anti-MRP4 rabbit polyclonal antibody and anti-CFTR mouse monoclonal antibody were used in the assay. Ezrin (*green*) is used as an apical marker of polarized HT29-CL19A cells (*left panel*). The *blue fluorescent dye* indicates nuclei. *AP*; apical side, *BL*; basolateral side. *F*, MRP4 was pulled down by GST-tagged PDZK1 from HT29-CL19A cells overexpressing MRP4. Irinotecan treatment led to increased interaction between MRP4 and PDZK1 in a dose-dependent manner. The bar graphs show the quantification of the data from blots in the pulldown assay. *G*, representative micrographs of PLA showing that MRP4 interacts with CFTR (*red dots* represent PLA signals) in enterospheres from $Mrp4^{+/+}$ mice. Irinotecan treatment increased PLA signals. Enterospheres from $Mrp4^{-/-}$ mice were used as a negative control. *H*, the bar graphs show the quantification of PLA signals from experiments as represented in *panel G*. The values represent the mean ± S.E. ($n \geq 3$ independent experiments in each group).

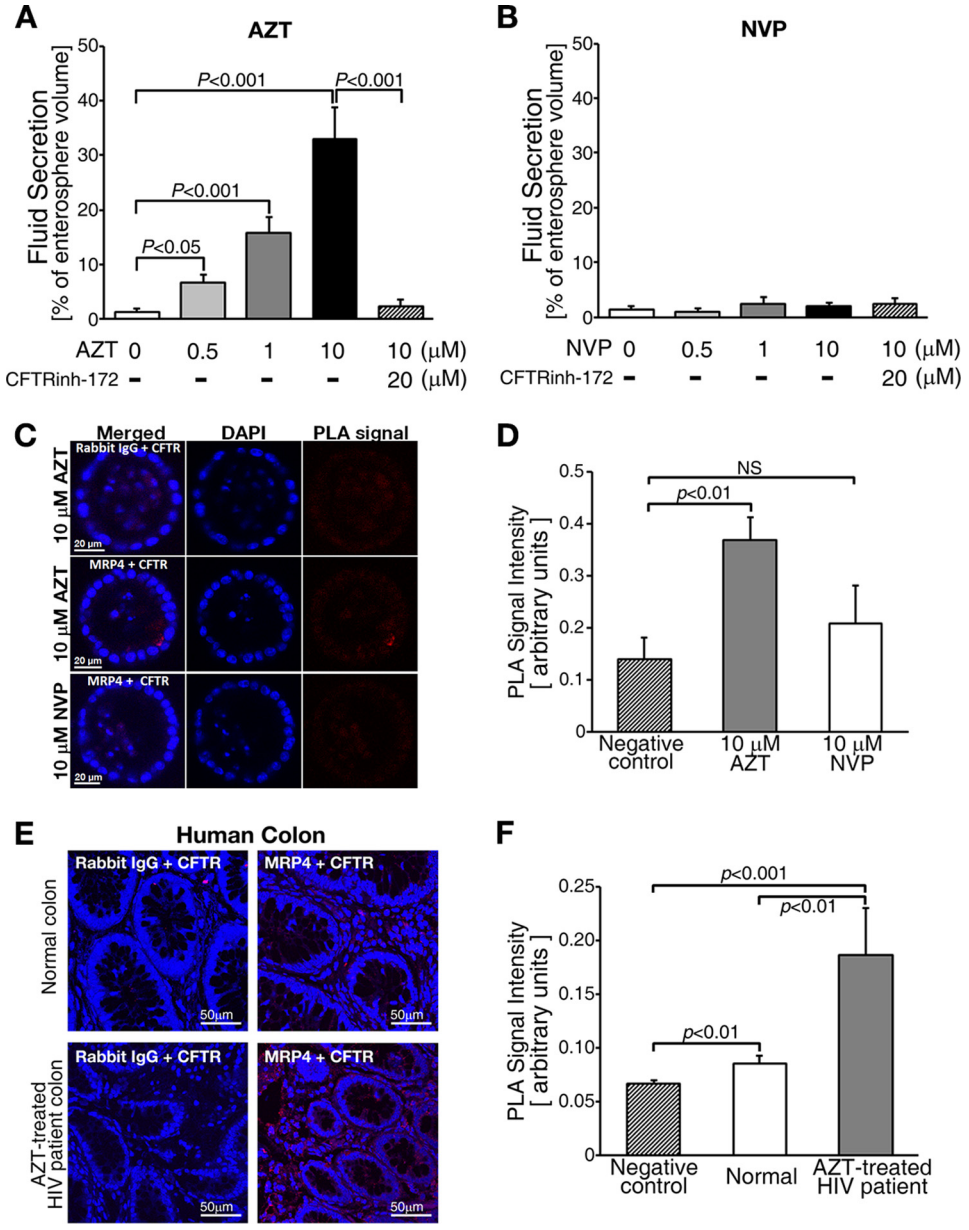

FIGURE 6. **An FDA-approved drug, AZT, enhanced the formation of MRP4-CFTR-containing macromolecular complexes at or near the plasma membrane.** *A*, AZT increased CFTR-mediated fluid secretion. *B*, a non-nucleoside reverse-transcriptase inhibitor, NVP, did not induce fluid secretion in enterospheres. The values represent the mean ± S.E. ($n \geq 5$ enterospheres per group). *C*, representative micrographs of the PLA signals (*red dots*) of MRP4-CFTR interaction in enterospheres from *Mrp4*$^{+/+}$ mice and those treated with AZT or NVP. PLA signals were increased in the AZT-treated enterospheres. Rabbit IgG was used as a negative control. *D*, the bar graphs show the quantification of PLA signals from experiments as represented in *panel C*. *NS*, not significant ($p \geq 0.05$). *E*, representative micrographs of PLA signals (*red dots*) of MRP4-CFTR interaction in human colon from a normal control and an AZT-treated HIV patient. PLA signals were increased in the AZT-treated HIV patient. Rabbit IgG was used as a negative control. *F*, the bar graphs show the quantification of PLA signals from experiments as represented in *panel E*. The values represent the mean ± S.E. ($n \geq 5$ enterospheres per group). *NS*, not significant ($p \geq 0.05$).

C–H). In contrast, forskolin, which activates adenylate cyclase, increased cAMP levels throughout the cell (Fig. 4, *E* and *F*). The compartmentalized elevation of cAMP levels would activate CFTR channels, provided that irinotecan does not disrupt the CFTR-MRP4-containing macromolecular complex at the plasma membrane. We found that irinotecan enhanced the formation of a multimolecular complex of CFTR and MRP4 mediated by PDZK1 at the plasma membrane. This was exemplified by the fact that MRP4 in the absence of irinotecan had higher lateral diffusion in the plasma membrane as measured by SPT (Fig. 4, *A* and *B*). However, in the presence of irinotecan, the mobility of MRP4 in the membrane was decreased, suggesting the clustering of MRP4 with CFTR in macromolecular complexes in mircodomains beneath the plasma membrane (Fig. 5).

Technically, our discovery is not narrowly confined to irinotecan-induced fluid secretion through compartmentalized cAMP and protein-protein interactions via PDZ motif. Diarrhea is a relatively frequent side effect accounting for ~7% of all adverse effects of drug use (1, 2). Thus, our findings have broad implications and may help to identify therapeutic targets for ameliorating medication-induced diarrheas. Here, we have demonstrated that an FDA-approved HIV/AIDS drug, AZT,

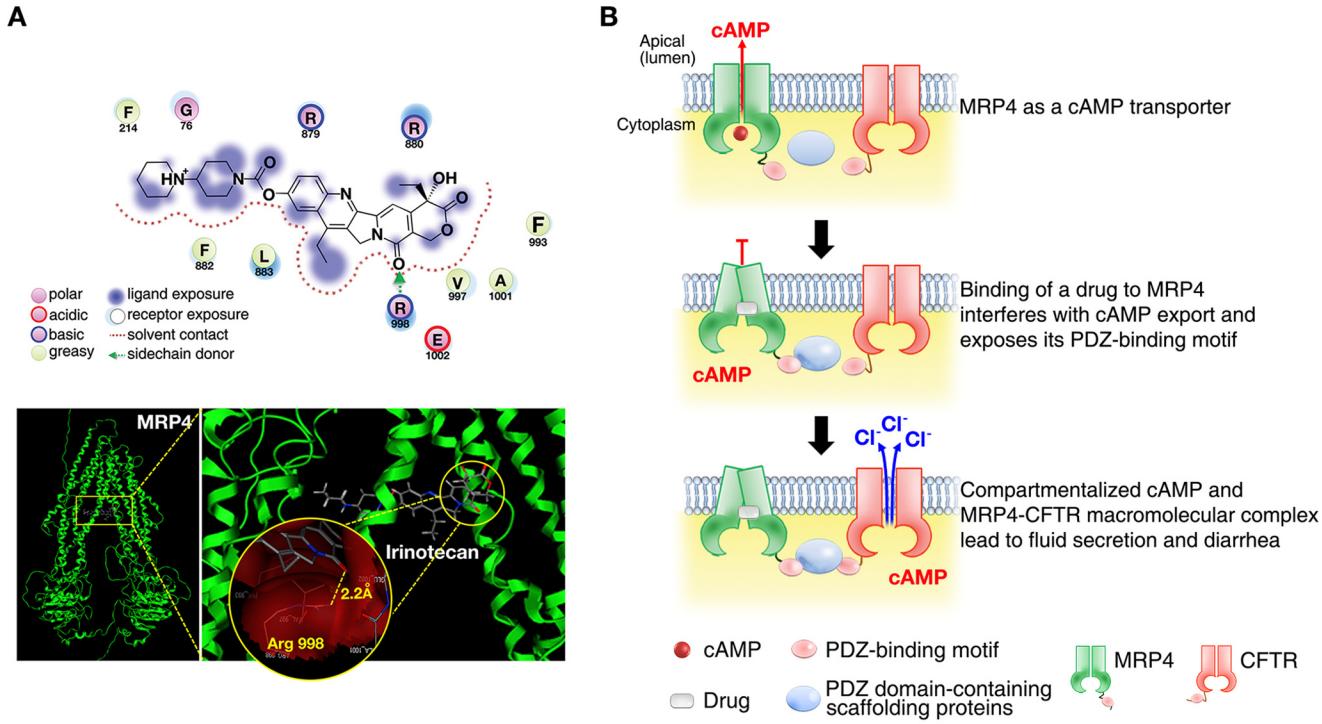

FIGURE 7. **Compartmentalized accumulation of cAMP and MRP4-CFTR-containing macromolecular complexes contributes to drug-induced diarrhea.** *A*, molecular interaction of irinotecan with MRP4. Irinotecan docked to MRP4 as expected, forming one hydrogen bond with the Arg-998 residue of 2.2 Å, and the conformation shows a docking score of −10.975 Kcal/mol (*upper panel*). *Left* and *right panels*, far (*left panel*) and close-up (*right panel*) views of docking poses of irinotecan in MRP4 (*lower panel*). The *yellow-dotted line* in the *circle* represents a hydrogen bond between irinotecan and MRP4. *Sticks* are colored according to atom type: carbon (*gray*), hydrogen (*dark gray*), oxygen (*red*), and nitrogen (*blue*). *B*, pictorial representation of a mechanism underlying the irinotecan-induced intestinal fluid secretion (and thus secretory diarrhea) through MRP4-coupled and CFTR-mediated protein-protein interactions. Binding of irinotecan to MRP4 changes MRP4 conformation into a closed pocket and exposes the PDZ motif of MRP4, impairing cAMP efflux across the plasma membrane and enhancing the formation of MRP4-CFTR-containing macromolecular complexes, which accumulates compartmentalized cAMP in proximity to CFTR and hyper-activates its channel function and ultimately causes secretory diarrhea.

increased fluid section by augmenting the formation of MRP4-CFTR-containing macromolecular complexes in both enterospheres and the colon of human HIV patients taking AZT (Fig. 6, *E* and *F*). To further explore the clinical relevance of our study, we tested the possibility of using tannic acid (1 mg/ml, which is a clinically relevant concentration) to mitigate intestinal fluid secretion in enterospheres from the mouse small intestine. Tannic acid is a potent radical scavenger and antioxidant (39) that has been reported to inhibit CFTR-induced intestinal fluid secretion. The antioxidant defense system in the small and large intestine in rats has been shown to be impaired in early chronic diarrhea (40). We found that tannic acid completely inhibited irinotecan-induced fluid secretion in mouse intestinal enterospheres (data not shown). Our data suggest that a medication regimen including an anti-diarrheal agent (*e.g.* tannic acid) may have benefits of reducing the diarrheal side effect and therefore improving the efficacy of drug therapy.

In summary, we have discovered a novel molecular mechanism by which irinotecan causes secretory diarrhea. We found that CFTR-MRP4-containing macromolecular complexes play an important role in the pathogenesis of drug-induced diarrhea. Our findings have important and broad clinical implications because our model system can be used in a high-throughput way to identify novel agents that can mitigate drug-induced diarrhea. Furthermore, our findings expand the notion that compartmentalized signaling (in this case, compartmentalized cAMP signaling) plays an important role in drug-induced pathophysiologic conditions such as drug-induced and CFTR-mediated secretory diarrheas.

Acknowledgments—We thank Dr. David Armbruster (Library, University of Tennessee Health Science Center, Memphis, TN), Jin Emerson-Cobb (Editorial Service, Memphis, TN), and J. Denise Wetzel (Cincinnati Children's Hospital Medical Center (CCHMC) Medical Writer) for critical review of our manuscript.

REFERENCES

1. Chassany, O., Michaux, A., and Bergmann, J. F. (2000) Drug-induced diarrhoea. *Drug Saf.* **22,** 53–72
2. Ratnaike, R. N., and Jones, T. E. (1998) Mechanisms of drug-induced diarrhoea in the elderly. *Drugs Aging* **13,** 245–253
3. Kunzelmann, K., and Mall, M. (2002) Electrolyte transport in the mammalian colon: mechanisms and implications for disease. *Physiol. Rev.* **82,** 245–289
4. Schuetz, J. D., Connelly, M. C., Sun, D., Paibir, S. G., Flynn, P. M., Srinivas, R. V., Kumar, A., and Fridland, A. (1999) MRP4: a previously unidentified factor in resistance to nucleoside-based antiviral drugs. *Nat. Med.* **5,** 1048–1051
5. Pizzolato, J. F., and Saltz, L. B. (2003) The camptothecins. *Lancet* **361,** 2235–2242
6. Maroun, J. A., Anthony, L. B., Blais, N., Burkes, R., Dowden, S. D., Dranitsaris, G., Samson, B., Shah, A., Thirlwell, M. P., Vincent, M. D., and Wong, R. (2007) Prevention and management of chemotherapy-induced diarrhea in patients with colorectal cancer: a consensus statement by the Canadian Working Group on Chemotherapy-Induced Diarrhea. *Curr. Oncol.* **14,** 13–20

7. Stein, A., Voigt, W., and Jordan, K. (2010) Chemotherapy-induced diarrhea: pathophysiology, frequency and guideline-based management. *Ther. Adv. Med Oncol.* **2,** 51–63
8. Blandizzi, C., De Paolis, B., Colucci, R., Lazzeri, G., Baschiera, F., and Del Tacca, M. (2001) Characterization of a novel mechanism accounting for the adverse cholinergic effects of the anticancer drug irinotecan. *Br. J. Pharmacol.* **132,** 73–84
9. Abdool Karim, Q., Abdool Karim, S. S., Frohlich, J. A., Grobler, A. C., Baxter, C., Mansoor, L. E., Kharsany, A. B., Sibeko, S., Mlisana, K. P., Omar, Z., Gengiah, T. N., Maarschalk, S., Arulappan, N., Mlotshwa, M., Morris, L., Taylor, D., and CAPRISA 004 Trial Group (2010) Effectiveness and safety of tenofovir gel, an antiretroviral microbicide, for the prevention of HIV infection in women. *Science* **329,** 1168–1174
10. Blandizzi, C., De Paolis, B., Colucci, R., Di Paolo, A., Danesi, R., and Del Tacca, M. (2001) Acetylcholinesterase blockade does not account for the adverse cardiovascular effects of the antitumor drug irinotecan: a preclinical study. *Toxicol. Appl. Pharmacol.* **177,** 149–156
11. Leggas, M., Adachi, M., Scheffer, G. L., Sun, D., Wielinga, P., Du, G., Mercer, K. E., Zhuang, Y., Panetta, J. C., Johnston, B., Scheper, R. J., Stewart, C. F., and Schuetz, J. D. (2004) Mrp4 confers resistance to topotecan and protects the brain from chemotherapy. *Mol. Cell. Biol.* **24,** 7612–7621
12. Ren, A., Zhang, W., Thomas, H. G., Barish, A., Berry, S., Kiel, J. S., and Naren, A. P. (2012) A tannic acid-based medical food, Cesinex®, exhibits broad-spectrum antidiarrheal properties: a mechanistic and clinical study. *Dig. Dis. Sci.* **57,** 99–108
13. Sato, T., Vries, R. G., Snippert, H. J., van de Wetering, M., Barker, N., Stange, D. E., van Es, J. H., Abo, A., Kujala, P., Peters, P. J., and Clevers, H. (2009) Single Lgr5 stem cells build crypt-villus structures *in vitro* without a mesenchymal niche. *Nature* **459,** 262–265
14. Ootani, A., Li, X., Sangiorgi, E., Ho, Q. T., Ueno, H., Toda, S., Sugihara, H., Fujimoto, K., Weissman, I. L., Capecchi, M. R., and Kuo, C. J. (2009) Sustained *in vitro* intestinal epithelial culture within a Wnt-dependent stem cell niche. *Nat. Med.* **15,** 701–706
15. McCracken, K. W., Howell, J. C., Wells, J. M., and Spence, J. R. (2011) Generating human intestinal tissue from pluripotent stem cells *in vitro*. *Nat. Protoc.* **6,** 1920–1928
16. Zeng, W., Lee, M. G., Yan, M., Diaz, J., Benjamin, I., Marino, C. R., Kopito, R., Freedman, S., Cotton, C., Muallem, S., and Thomas, P. (1997) Immuno and functional characterization of CFTR in submandibular and pancreatic acinar and duct cells. *Am. J. Physiol.* **273,** C442–C455
17. Penmatsa, H., Zhang, W., Yarlagadda, S., Li, C., Conoley, V. G., Yue, J., Bahouth, S. W., Buddington, R. K., Zhang, G., Nelson, D. J., Sonecha, M. D., Manganiello, V., Wine, J. J., and Naren, A. P. (2010) Compartmentalized cyclic adenosine 3′,5′-monophosphate at the plasma membrane clusters PDE3A and cystic fibrosis transmembrane conductance regulator into microdomains. *Mol. Biol. Cell* **21,** 1097–1110
18. Li, C., Krishnamurthy, P. C., Penmatsa, H., Marrs, K. L., Wang, X. Q., Zaccolo, M., Jalink, K., Li, M., Nelson, D. J., Schuetz, J. D., and Naren, A. P. (2007) Spatiotemporal coupling of cAMP transporter to CFTR chloride channel function in the gut epithelia. *Cell* **131,** 940–951
19. Dahan, M., Lévi, S., Luccardini, C., Rostaing, P., Riveau, B., and Triller, A. (2003) Diffusion dynamics of glycine receptors revealed by single-quantum dot tracking. *Science* **302,** 442–445
20. Söderberg, O., Leuchowius, K. J., Gullberg, M., Jarvius, M., Weibrecht, I., Larsson, L. G., and Landegren, U. (2008) Characterizing proteins and their interactions in cells and tissues using the in situ proximity ligation assay. *Methods* **45,** 227–232
21. Vilar, S., Cozza, G., and Moro, S. (2008) Medicinal chemistry and the molecular operating environment (MOE): application of QSAR and molecular docking to drug discovery. *Curr. Top. Med. Chem.* **8,** 1555–1572
22. Vilar, S., González-Díaz, H., Santana, L., and Uriarte, E. (2008) QSAR model for alignment-free prediction of human breast cancer biomarkers based on electrostatic potentials of protein pseudofolding HP-lattice networks. *J. Comput. Chem.* **29,** 2613–2622
23. Damu, A. G., Jayaprakasam, B., Rao, K. V., and Gunasekar, D. (1998) A flavone glycoside from *Andrographis alata*. *Phytochemistry* **49,** 1811–1813
24. Sato, T., van Es, J. H., Snippert, H. J., Stange, D. E., Vries, R. G., van den Born, M., Barker, N., Shroyer, N. F., van de Wetering, M., and Clevers, H. (2011) Paneth cells constitute the niche for Lgr5 stem cells in intestinal crypts. *Nature* **469,** 415–418
25. Stelzner, M., Helmrath, M., Dunn, J. C., Henning, S. J., Houchen, C. W., Kuo, C., Lynch, J., Li, L., Magness, S. T., Martin, M. G., Wong, M. H., and Yu, J. (2012) A nomenclature for intestinal *in vitro* cultures. *Am. J. Physiol. Gastrointest. Liver Physiol.* **302,** G1359–G1363
26. Liu, J., Walker, N. M., Cook, M. T., Ootani, A., and Clarke, L. L. (2012) Functional Cftr in crypt epithelium of organotypic enteroid cultures from murine small intestine. *Am. J. Physiol. Cell Physiol.* **302,** C1492–C1503
27. Barker, N., van Es, J. H., Kuipers, J., Kujala, P., van den Born, M., Cozijnsen, M., Haegebarth, A., Korving, J., Begthel, H., Peters, P. J., and Clevers, H. (2007) Identification of stem cells in small intestine and colon by marker gene *Lgr5*. *Nature* **449,** 1003–1007
28. Sangiorgi, E., and Capecchi, M. R. (2008) *Bmi1* is expressed *in vivo* in intestinal stem cells. *Nat. Genet.* **40,** 915–920
29. Pavlov, O. G., and Ovsiannikov, V. I. (1987) [Contractile reactions of the small intestine induced by stimulation of β-adrenoreceptors]. *Fiziol. Zh. SSSR Im. I. M. Sechenova* **73,** 517–523
30. Schaaf, L. J., Hammond, L. A., Tipping, S. J., Goldberg, R. M., Goel, R., Kuhn, J. G., Miller, L. L., Compton, L. D., Cisar, L. A., Elfring, G. L., Gruia, G., McGovren, J. P., Pirotta, N., Yin, D., Sharma, A., Duncan, B. A., and Rothenberg, M. L. (2006) Phase 1 and pharmacokinetic study of intravenous irinotecan in refractory solid tumor patients with hepatic dysfunction. *Clin. Cancer Res.* **12,** 3782–3791
31. Sparreboom, A., de Jonge, M. J., de Bruijn, P., Brouwer, E., Nooter, K., Loos, W. J., van Alphen, R. J., Mathijssen, R. H., Stoter, G., and Verweij, J. (1998) Irinotecan (CPT-11) metabolism and disposition in cancer patients. *Clin. Cancer Res.* **4,** 2747–2754
32. Kool, M., de Haas, M., Scheffer, G. L., Scheper, R. J., van Eijk, M. J., Juijn, J. A., Baas, F., and Borst, P. (1997) Analysis of expression of *cMOAT* (*MRP2*), *MRP3*, *MRP4*, and *MRP5*, homologues of the multidrug resistance-associated protein gene (*MRP1*), in human cancer cell lines. *Cancer Res.* **57,** 3537–3547
33. Tian, Q., Zhang, J., Tan, T. M., Chan, E., Duan, W., Chan, S. Y., Boelsterli, U. A., Ho, P. C., Yang, H., Bian, J. S., Huang, M., Zhu, Y. Z., Xiong, W., Li, X., and Zhou, S. (2005) Human multidrug resistance associated protein 4 confers resistance to camptothecins. *Pharm. Res.* **22,** 1837–1853
34. Sager, G., and Ravna, A. W. (2009) Cellular efflux of cAMP and cGMP: a question about selectivity. *Mini. Rev. Med. Chem.* **9,** 1009–1013
35. Dallas, S., Schlichter, L., and Bendayan, R. (2004) Multidrug resistance protein (MRP) 4- and MRP 5-mediated efflux of 9-(2-phosphonylmethoxyethyl)adenine by microglia. *J. Pharmacol. Exp. Ther.* **309,** 1221–1229
36. Li, C., and Naren, A. P. (2010) CFTR chloride channel in the apical compartments: spatiotemporal coupling to its interacting partners. *Integr. Biol. (Camb.)* **2,** 161–177
37. Seidler, U., Singh, A. K., Cinar, A., Chen, M., Hillesheim, J., Hogema, B., and Riederer, B. (2009) The role of the NHERF family of PDZ scaffolding proteins in the regulation of salt and water transport. *Ann. N.Y. Acad. Sci.* **1165,** 249–260
38. Max, B., and Sherer, R. (2000) Management of the adverse effects of antiretroviral therapy and medication adherence. *Clin. Infect. Dis.* **30,** Suppl. 2, S96–S116
39. Riedl, K. M., and Hagerman, A. E. (2001) Tannin-protein complexes as radical scavengers and radical sinks. *J. Agric. Food Chem.* **49,** 4917–4923
40. Nieto, N., López-Pedrosa, J. M., Mesa, M. D., Torres, M. I., Fernández, M. I., Ríos, A., Suárez, M. D., and Gil, A. (2000) Chronic diarrhea impairs intestinal antioxidant defense system in rats at weaning. *Dig. Dis. Sci.* **45,** 2044–2050